JOC The Journal of Organic Chemistry

Article

pubs.acs.org/joc

Mechanistic Diversity in Thermal Fragmentation Reactions: A Computational Exploration of CO and CO_2 Extrusions from Five-Membered Rings

Henry S. Rzepa*,† and Curt Wentrup*,‡

†Department of Chemistry, Imperial College London, South Kensington Campus, London SW2 2AZ, U.K.

‡School of Chemistry and Molecular Biosciences, The University of Queensland, Brisbane, Queensland 4072, Australia

Supporting Information

ABSTRACT: The mechanisms of a variety of thermal pericyclic fragmentation reactions of five-membered heterocyclic rings are subjected to scrutiny at a density functional level by computation of transition state free energy barriers and intrinsic reaction coordinates (IRCs). The preferred computed products generally match those observed in flash vacuum thermolysis experiments. For certain reactions, which also have the highest reaction temperatures and computed barriers, a degree of multireference character to the wave function manifests in an overestimation of the DFT-computed barrier, with a more reasonable barrier obtained by a CASSCF single point energy calculation. Many of the IRCs exhibit "hidden intermediates" along the reaction pathway, but conversely reactions that could be considered to involve the formation of an intermediate nitrene prior to alkyl or aryl migration show no evidence of such an intermediate. Such exploration of the diversity of behavior in a class of compounds using computational methods with interactive presentation of the results within the body of a journal article is suggested as being almost a *sine qua non* for laboratory-based research on reactive intermediates.

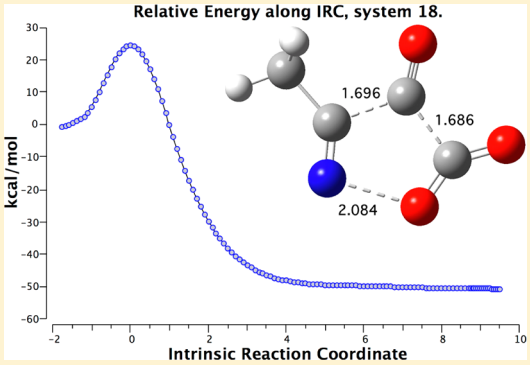

INTRODUCTION

A wide range of pericyclic fragmentation reactions of five-membered heterocyclic compounds are known, many of which are useful synthetically using flash vacuum thermolysis (FVT). The outcomes of these reactions can be determined in a quite subtle manner by the nature of the heteroatoms present, either in the ring itself, or *exo* to it. In this article we set out to subject selected examples of these reactions to computational mechanistic scrutiny, the objective being 2-fold: (a) to identify a thermally reasonable route for each type of fragmentation and (b) using this class of reaction as a "reality check" to establish the feasibility of mechanistic prototyping via reasonably accurate quantum mechanical procedures.

Overview of Fragmentation Diversity. The cheletropic extrusion of CO from furan- thiophen- and pyrrole-2,3-diones **1**−**3** is a convenient method of synthesis of acyl-, thioacyl-, and imidoylketenes **4**−**6** (Scheme 1).[1] The furandiones are the most reactive, decomposing already at 120 °C in solution or in the neat solid state, or at 250 °C under the conditions of FVT. The thiophendiones and pyrrolediones decompose at ca. 200−250 °C in condensed phases, or above 300 and 500 °C, respectively, on FVT.[1] In a similar way, 4-methyleneoxazolones (azlactones) **7** extrude CO to form *N*-acylketenimines **8** in good yields on FVT at 600 °C.[2]

Pyrazole-4.5-diones **9** were thus expected to follow the same pattern to yield azoketenes **10**. Instead, the reaction took a different mechanistic course on FVT at 750 °C, resulting in fragmentation to phenyl isocyanate **11**, MeCN and CO instead (Scheme 1).[3] Replacement of one ring nitrogen in **9** by an oxygen to give 4-substituted isoxazol-5(4*H*)-ones **12** results in an analogous fragmentation to CO_2, RCN and a vinylidene-type species Z═C: **14**. Cheletropic extrusion of CO to form nitrosoketenes **13** is never observed.[4] We may speculate at this stage that the differing behavior of the pyrazolones and isoxzolones may be due to the presence of the relatively weak N−N and N−O bonds, respectively, the thermal cleavage of which could generate species such as **15** followed by cyclization to azirenes **16**. The latter may be in equilibrium with vinylnitrenes **17**.[5,6] Further fragmentation can now generate CO_2, a nitrile, and the species Z═C: **14**. For Z = O, this reaction is extremely facile, so much so that diones **18** are not isolable at room temperature, fragmenting to CO_2, CO, and RCN on attempted synthesis. The imines **19** are stable, crystalline compounds, but they fragment readily to isocyanides R′−NC **20** at 90−110 °C, e.g., in toluene solution (Scheme 1).[7,8]

Similar diversity is found for FVT of 4-methylene-5(4*H*)-isoxazolones **21**. This is a high-yielding method for the synthesis of aryl- and heteroarylacetylenes such as **25** (Scheme 2).[9,10] Ring-opening with CO_2 loss may lead to vinylnitrenes **22**,

Received: May 24, 2013
Published: June 24, 2013

   dx.doi.org/10.1021/jo401146k | J. Org. Chem. 2013, 78, 7565−7574

Scheme 1

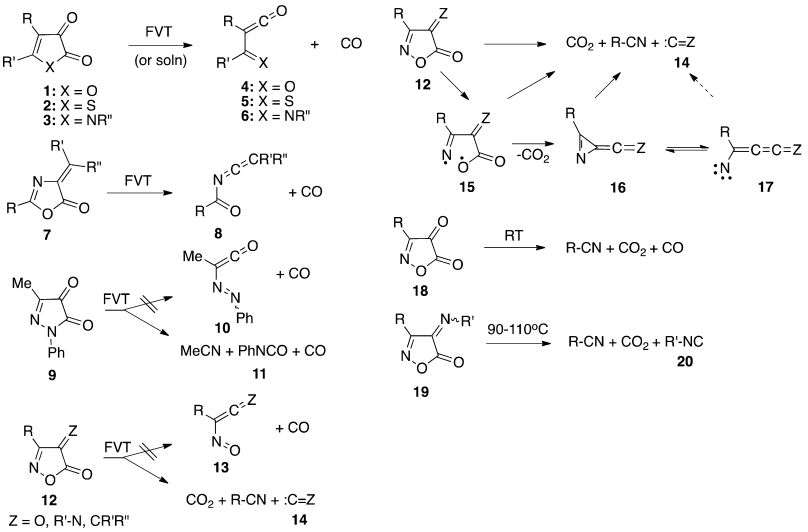

Scheme 2

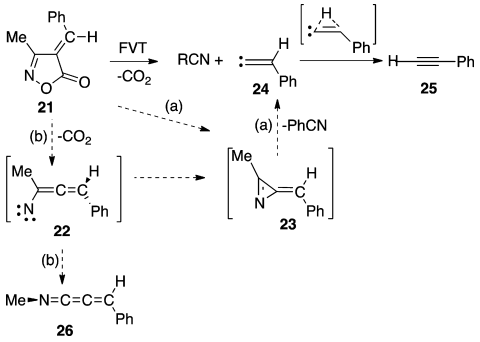

azirenes **23** and vinylidenes **24** (cf. Z═C: **14** in Scheme 1). 1,2-Shifts in vinylidenes are known to furnish acetylenes with low activation barriers.[11] In view of other cumulene-forming rearrangements described below, a formation of propadienylideneimine **26** could have been expected but was not observed, and it is unclear whether the reaction may proceed via intermediates such as nitrene **22** and/or azirene **23** (Scheme 2).

The 3-methyl-4-[bis(methylthio)methylene]isoxazolone **29** affords bis(methylthio)ethyne **28** on FVT, presumably via the vinylidene **27** (Scheme 3). The 3-phenyl derivative **29** also affords ethyne **28**, but, in addition, there is evidence in this case from collisional activation mass spectrometry (CAMS) for formation of either azirene **31** or cumulene **32** (*m*/*z* 221).

Scheme 3

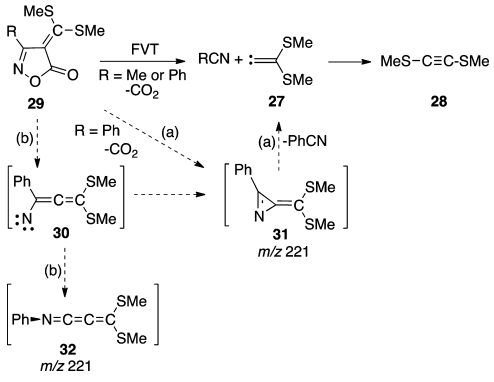

The thioketene **33** can be generated by FVT of the bis(methylthio) isoxazolone **29** or more efficiently from the analogous bis(ethylthio) or bis(isopropylthio) derivatives. Thioketene **33** may ring open to nitrene **34** and/or azirene **35**. A 1,2-phenyl shift generates the cumulene **36**, PhNCCCS, which is obtained in high yield (Scheme 4).[12]

Scheme 4

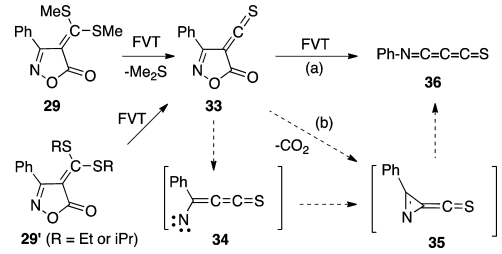

Scheme 5

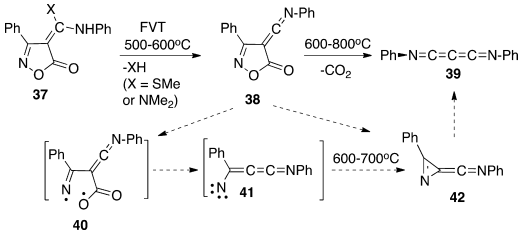

The 4-(arylaminomethylene)isoxazolones **37** are excellent precursors of bisiminopropadienes **39** by FVT (Scheme 5).[13] Here, there is strong experimental evidence from matrix-IR and CAMS that ketenimines **38** are formed first, at the mildest FVT temperatures (500−600 °C). At higher temperatures, 600−800 °C, the bisimines **39** are obtained cleanly. At intermediate temperatures, ca. 600−700 °C, a third species with the same mass as **39** and assigned as the azirene **42** is formed, but due to the narrow temperature interval, it was not possible to obtain this compound cleanly.[15] Diradical **40** and nitrene **41** may be transient, unobserved, intermediates (Scheme 5).

The Computational Objectives. The five schemes above illustrate the richness and diversity of the chemistry of these small rings. A coherent picture of this chemistry emerges when coupled

dx.doi.org/10.1021/jo401146k | J. Org. Chem. 2013, 78, 7565−7574

Table 1. Thermochemical Data for Reactions[a]

system	$\Delta G^{\ddagger}_{298}$[b]
	23.1 (1: R = H, R′ = Me) [S][c]
	37.9 (2: R = H, R′ = Me) [S]
	27.7 (3: R = H, R′ = Me) [S]
7	49.5 (7: R = Me, R′ = H, R″ = Ph) [S]
	58.7 (7: R = Me, R′ = R″ = SCH_2CH_2S) [S]
	74.0 (7: R = Me, R′ = R″ = SCH_2CH_2S) lactone [S]
9	51.8 [S]
	47.8 (alt) [S]
18	21.8 CO + CO_2 Loss [S]
	43.7 CO Loss [S]
19	33.5 (R = Me) [S]
	59.5 (R = ME) CO Loss [S]
21	21: R = Me, 67.2 [S]
	21: R = Me, 64.9 (61.4 at 1000 K) [U, −5.7]
	21: R = Me, 45.2
	21: R = Me, 39.0
	50: R = Ph, 54.8 [S]
	50: R = Ph, 64.3 [U, −9.1]
29	56.2 (29, Migration) [S]
	62.1 (29, Azirene) [U, −9.6]
	34.3 (29, Vinylidene elim) [S]
33	X = S, R = Me: 55.5 (49.4 at 1000 K)
	X = S, R = Ph: 53.3 (48.3 at 1000 K) [S]
	X = S, R = Ph: 69.3 [U, −12.0]
38	56.7 (Ph migration) [S]
	69.9 (Azirene formation) [U, −12.2]
	28.1 Azirene, ring open
	29.1 Azirene, loss of CO_2

[a]Coordinates of all the systems and animations of intrinsic reaction coordinates, together with energies (hyperlinked to a complete OAI-PMH compliant digital repository entry containing full details of each calculation) are available via the Web-enhanced object version of this table. A Java-enabled Web browser is required to view the 3D models. [b]Calculated using Gaussian 09, revision C.01, at the ωB97XD DFT levels and the 6-311G(d,p) basis set, using an ultrafine grid. Energies relative to reactant in kcal mol^{-1}. The intrinsic reaction coordinates (IRC) are computed with the following parameters: **maxpoints=150,recalc=5,calcfc,maxcycle=40,tight,cartesian**. [c]Wave function stability (Gaussian keyword STABLE): S = stable to open shell configurations, or U = unstable + value of lowest open shell triplet state in kcal/mol relative to the close shell singlet.

Chart 1. Reactants Selected for Computational Exploration[a]

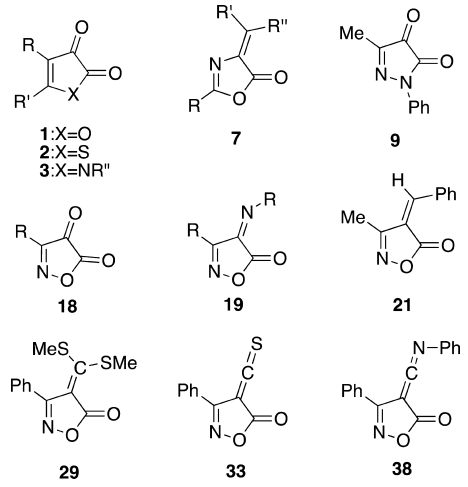

[a]The contexts for **1**, **7**, **9**, **18**, and **19** are to be found in Scheme 1, those for **21**, **29**, and **33** in Schemes 2, 3, and 4, and those for **38** in Scheme 5.

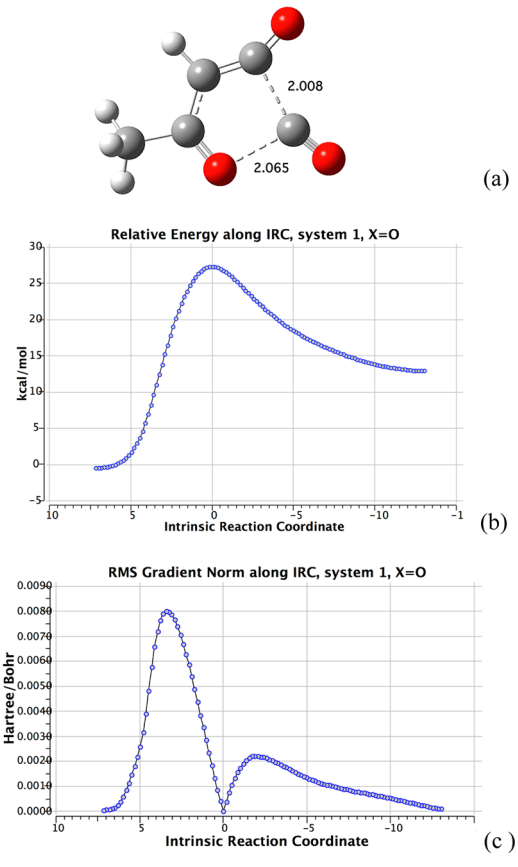

Figure 1. Transition state geometry (a), energy profile (b), and associated RMS gradient norm (c) along the reaction pathway for **1** (X = O) computed at the ωB97XD/6-311G(d,p) level.

with mechanistic speculation about how the different behaviors arise. For molecules of this size, it is however nowadays possible to augment such informed speculation with a more quantitative assessment of the viability or otherwise of the proposed routes in terms of computed reaction barriers and intrinsic reaction coordinate pathways based on the identified transition states in the potential energy surface. Of equal interest is the ability to compare at a consistent level the profiles of reactions with different substituents, or varying types of ring.

The computational task to be undertaken is certainly simplified because all these reactions occur in the gas phase, without the need for a mediating solvent. In this study, the ωB97XD DFT procedure has been selected.[14] This is a relatively recent functional, which was specifically developed for modeling reaction kinetics, and it also incorporates a correction for dispersion terms. The latter is probably an essential component for exploring a wider range of the potential energy surface via computation of an intrinsic reaction coordinate. A medium quality basis set 6-311G(d,p) was selected as suitable for reasonably high throughput exploration of a range of reactions and their associated intrinsic reaction coordinate (IRC) profiles. Transition states were located and characterized with a single negative force constant in the Hessian matrix, and the wave function at this geometry was subjected to a stability test with respect to open shell UHF states. 3D coordinates and vibration

dx.doi.org/10.1021/jo401146k | J. Org. Chem. 2013, 78, 7565−7574

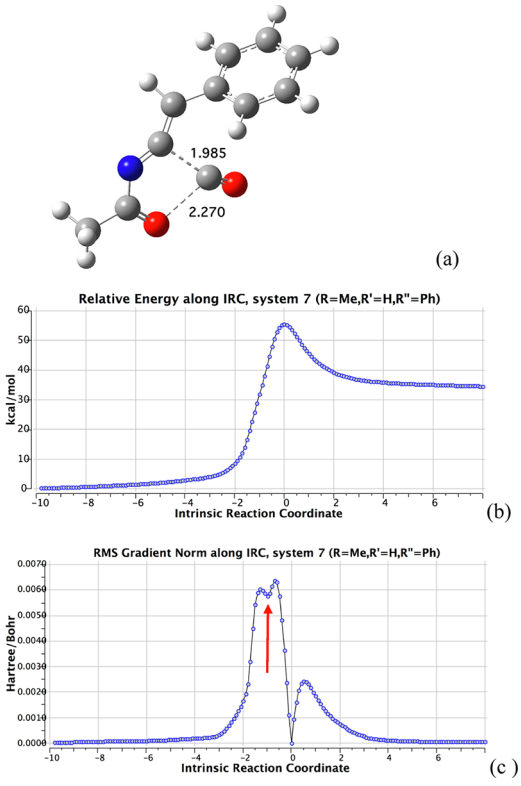

Figure 2. Transition state geometry (a), energy profile (b), and associated RMS gradient norm (c) along the reaction pathway for **7** (R = Me, R′ = H, R″ = Ph) computed at the ωB97XD/6-311G(d,p) level. The arrow points to a "hidden intermediate" (see text).

and reaction animations can be viewed via an interactive table (Table 1).

With access to modern computer resources, the workflow reported here can be achieved in about two months of elapsed time, which compares favorably with the laboratory time involved in conducting the reactions. Two further tools are here deployed to facilitate access to the computational results. First, a complete and open archive of each calculation is created in the form of a digital repository.[15] The data in such a repository is fully validated, with complete details added in the form of formal metadata, and the fileset for each calculation is assigned a digital object identifier (doi) at time of deposition. This places the data associated with this article on an equal footing with the article itself; both have an assigned doi that can be easily used to retrieve the information. In this instance, the repository links are to the Figshare system, which is a modern open-access repository in which all the objects are on unrestricted access.[16] Each item is also duplicated in another repository based on the DSpace system.[15] The second feature is the inclusion of what we call an "interactivity box" as a principle component of the HTML version of this article. This ensures that an interactive model of the modeled species is immediately accessible to the reader, along with animations of the reaction coordinates and other information. Whitesides[17] has argued recently that the accessibility of the standard scientific publication should be enhanced with such animations to improve a reader's assimilation of the concepts being presented.

RESULTS AND DISCUSSION

For convenience, the systems studied are summarized in Chart 1 with the corresponding data in Table 1 (print summary and Web-enhanced interactive version in the Supporting Information,

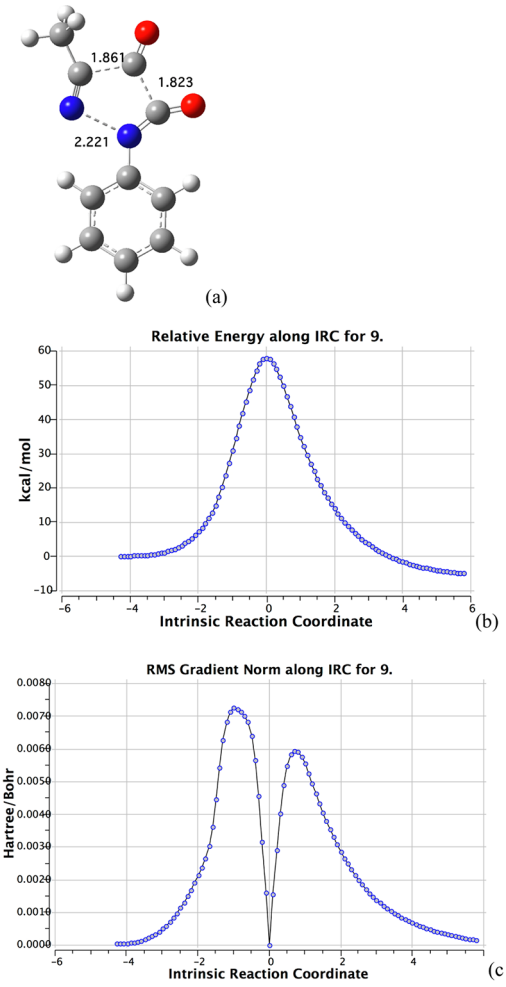

Figure 3. Transition state geometry (a), energy profile (b), and associated RMS gradient norm (c) along the reaction pathway for **9** computed at the ωB97XD/6-311G(d,p) level.

including coordinates, animations and links to digital repository entries for further information).

Systems 1−3 (Scheme 1). It was noted above that **1** (X = O) fragments readily at relatively low temperatures, while the thio and aza analogues require slightly higher temperatures. The computed free energy barriers ΔG_{298} for these systems accurately reflect this behavior, that for **1** (X = O) being in the range for a reaction occurring below 120 °C, with the aza-analogue higher and the thio system highest in activation energy. The full force constant matrix and geometry for computing the free energy barrier at other temperatures is available via the digital repository entry cited in the interactive table. An intrinsic reaction coordinate (IRC) computation shows this to be a smoothly concerted and also synchronous cheletropic elimination of CO (Figure 1a), with a closed shell wave function at the transition state. The IRC corroborates the straightforward nature of the potential energy surface.

System 7 (Scheme 1). The azlactone **7** undergoes a similar CO extrusion, albeit at an FVT temperature of ∼600 °C, which suggests a higher barrier than observed for **1**−**3**. The calculations both confirm the increased barrier and reiterate the closed shell character of the reaction. Another difference is the greater asymmetry of the two cleaving bond lengths at the transition state (Figure 2), along with a new feature in the IRC profile (marked with an arrow against the gradient norm) just prior to

dx.doi.org/10.1021/jo401146k | J. Org. Chem. 2013, 78, 7565−7574

the transition state. This (small) dip in the gradient norm hints at the incursion of what is termed a hidden intermediate[18] in the reaction, a species that might resemble in its valence bond structure a potentially viable stable geometry. A hidden intermediate, which would not be expected to have a lifetime of more than a molecular vibration, could potentially be converted into a real intermediate with a longer lifetime if the conditions or substitution pattern are changed.[18] At this geometry, the C−C and C−O lengths for **7** are respectively 1.506 and 1.894 Å, which suggest that just prior to the transition state, some charge separated zwitterionic character develops, although it is removed again as the profile passes the transition state and CO becomes fully eliminated. This change in character is induced by the nitrogen atom in the ring and the change from an *exo*-carbonyl to an *exo*-alkene.

System 9 (Scheme 1). This combination retains the *exo*-carbonyl from **7**, but introduces a weak N−N bond into the ring. The FVT requires a slightly higher temperature than for **7**, with the previous outcome of CO extrusion but now with further fragmentation occurring to cleave the weak N−N bond and give MeCN and PhNCO. No formation of **10** was observed. A closed-shell transition state corresponding to this as a concerted process (Figure 3) reveals the N···N bond to asynchronously break first, with the C−C and C−O bond lengths of the extruding CO still largely intact at this stage and with a free energy activation barrier similar to that for **7**. The IRC is relatively dull, showing no hidden (charge-separated) intermediates attempting to form on the pathway, and reveals the reaction is slightly exothermic in enthalpy with a negative free energy ΔG of reaction (−21.6 kcal/mol) resulting from the large increase in entropy.

It also proved possible to locate an alternate transition state with an intact N−N bond corresponding to CO elimination to give **10** rather than fragmentation. This emerged as 4.0 kcal/mol lower in free energy (Figure 4) but 28.2 kcal/mol endothermic for ΔG in comparison to **9**, with only a small (14 kcal/mol) reverse barrier. It seems unlikely, however, that the conditions of a low pressure FVT experiment would allow for thermodynamic rather than kinetic product control, and so this calculation could be flagged for further attention such as improved basis set or correlation treatment. Since the N−N bond breaks early (Figure 3), the reaction is predestined to lead to PhNCO, and the dynamics mitigate against a reversal to the pathway yielding CO and the azoketene.

System 18 (Scheme 1). This represents another apparently minor change from **1**−**3**, with a simple replacement of C for N in the ring, thus introducing a weak N−O bond. This change suppresses exclusive CO extrusion, replacing it instead with CO_2 elimination and resulting also in formation of CO. The transition states for both processes can be located, with the barrier to the observed (highly exothermic) fragmentation being very much lower (21.8 kcal/mol) than that for the suppressed reaction (Table 1), and with a value that corresponds to the observed decomposition at room temperatures of **18** upon attempted preparation. The IRC profile is again relatively featureless (Figure 5).

System 19 (Scheme 1). In contrast to **18**, which is not stable at ambient temperatures, **19** can be prepared as a crystalline substance. Commensurate with this, the barrier calculated for N−O cleavage (Figure 6) is rather higher (33.5 kcal/mol),

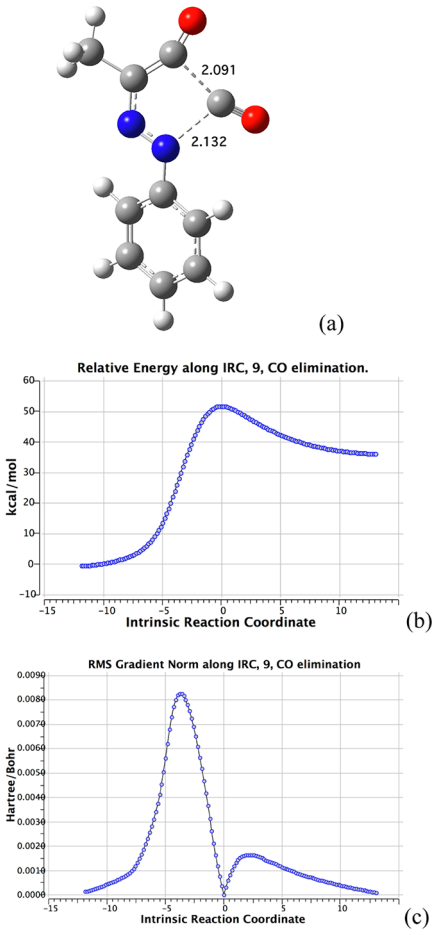

Figure 4. Transition state geometry (a), energy profile (b), and associated RMS gradient norm (c) along the reaction pathway of **9** for CO elimination, computed at the ωB97XD/6-311G(d,p) level.

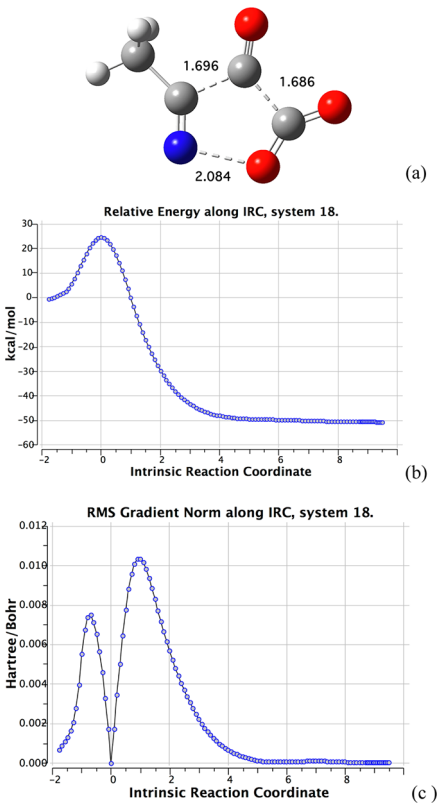

Figure 5. Transition state geometry (a), energy profile (b), and associated RMS gradient norm (c) along the reaction pathway for **18** for CO_2 elimination, computed at the ωB97XD/6-311G(d,p) level.

dx.doi.org/10.1021/jo401146k | J. Org. Chem. 2013, 78, 7565−7574

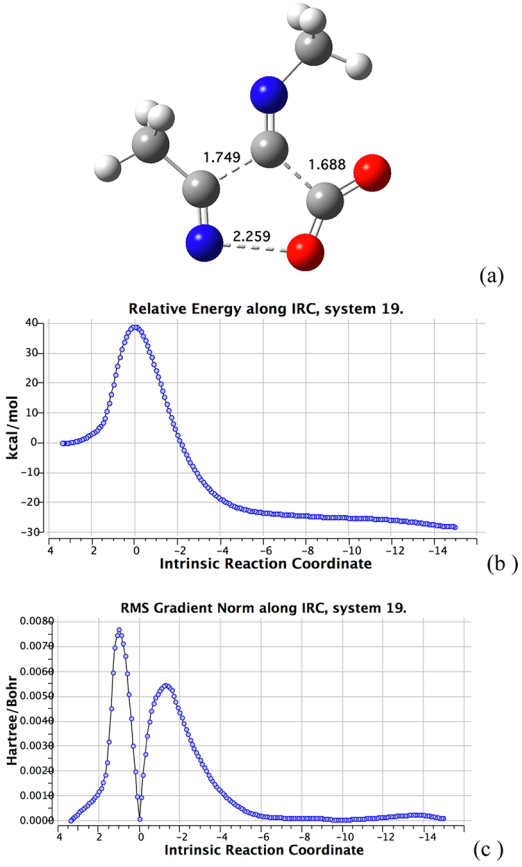

Figure 6. Transition state geometry (a), energy profile (b), and associated RMS gradient norm (c) along the reaction pathway for **19** for CO_2 elimination, computed at the ωB97XD/6-311G(d,p) level.

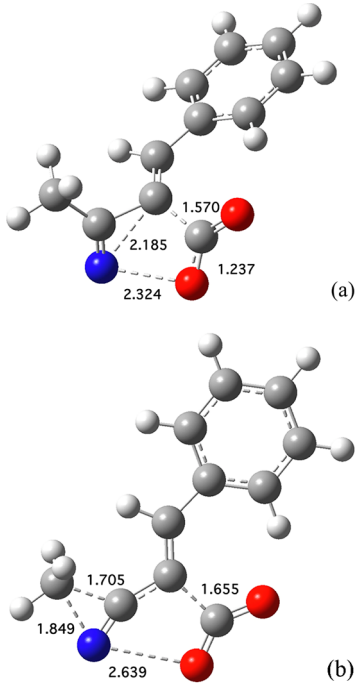

Figure 7. Transition state geometry for (a) azirene **23** formation from **21**, (b) methyl group migration, computed at the ωB97XD/6-311G(d,p) level.

but compatible with the observed temperatures for the formation of isocyanides (90−110 °C).

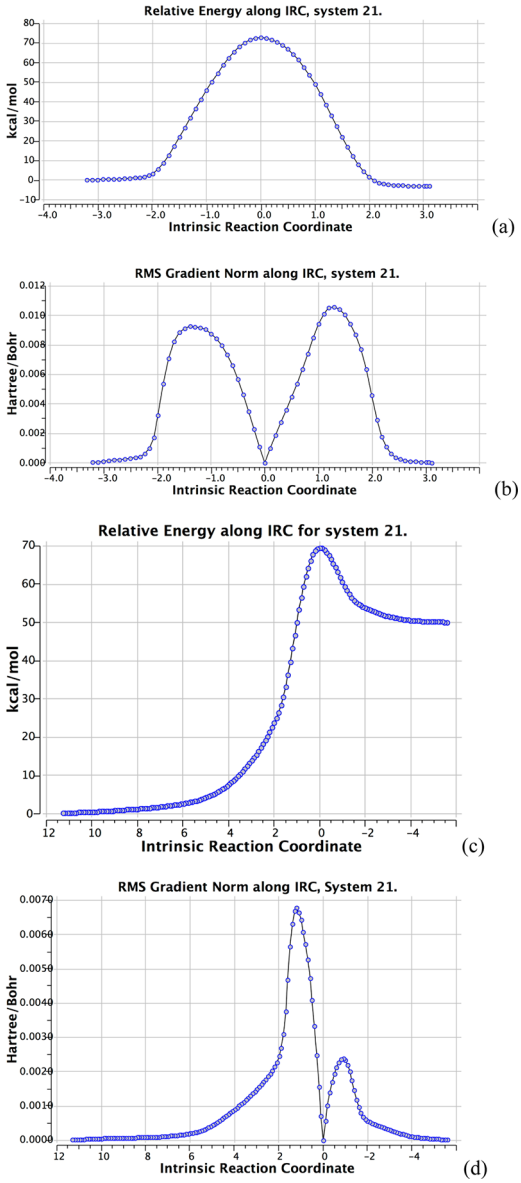

Figure 8. IRC profiles for **21**, (a) and (b) methyl migration to **26**; (c) and (d) formation of azirene **23**, computed at the ωB97XD/6-311G(d,p) level.

System 21 (Scheme 2). This series of reactions represents a different type of diversity in which the imine group on **19** is replaced by a vinylic carbon. Species **21** has two quite different channels for reaction. The first (Figure 7a) is a more subtle pericyclic process, formally at least corresponding to a 4-electron cycloelimination to form a N−C bond, with a barrier of 64.9 kcal/mol (61.4 at 1000 K) forming an azirene **23** (Scheme 2). Route a is the reaction actually observed experimentally, leading to the alkyne product **25**. The second route (Figure 7b) involves cleavage of the weak O−N bond with concerted migration of R to give the unobserved aza-cumulene Me-NCCZ **26**, with a computed barrier of 67.2 kcal/mol.

These reactions occur at FVT temperatures of up to 1000 K. If the residency time in which the sample is exposed to this temperature is typically taken as ∼0.002s, using the expression $\ln k/T = 23.76 - \Delta G/RT$ to relate a free energy barrier to a rate constant (half-life) gives an experimental estimate of the free energy barrier of ∼50 kcal/mol at this temperature.

dx.doi.org/10.1021/jo401146k | J. Org. Chem. 2013, 78, 7565−7574

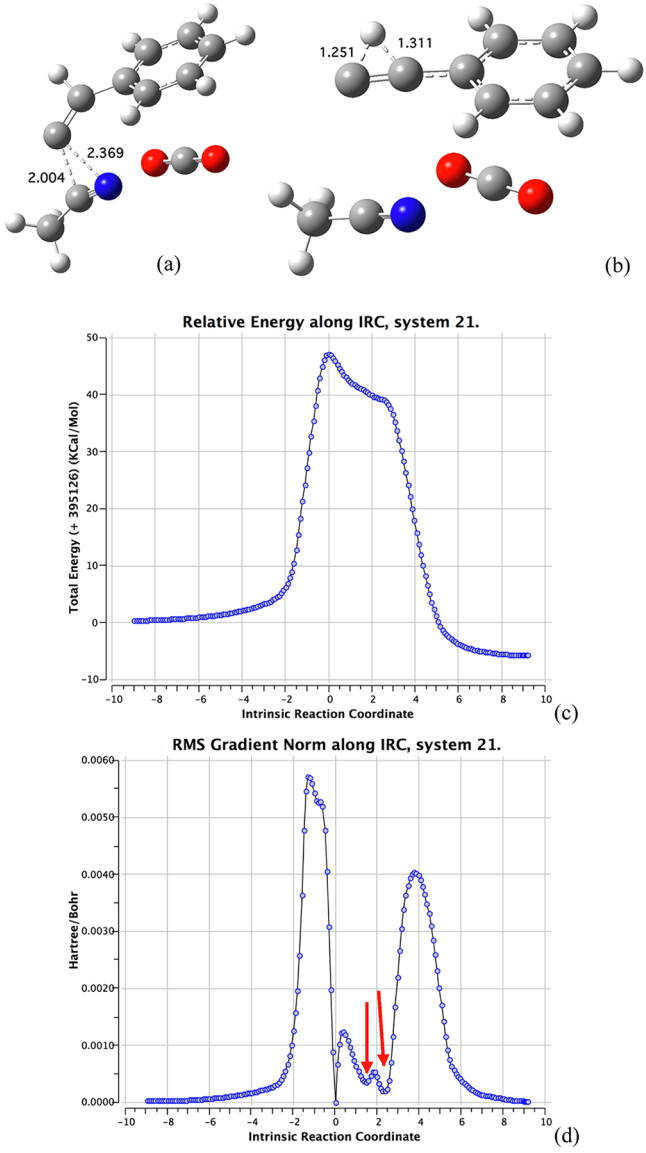

Figure 9. (a) Transition state geometry for fragmentation of **21**; (b) geometry of the "hidden intermediate" corresponding to a 1,2-H shift in vinylidene **24**; (c) and (d) IRC profiles: in (d) the red arrows point to "hidden intermediates" for fragmentation of **21** to give azirene **23**, followed by a [1,2]-hydrogen migration in vinylidene **24** to produce alkyne **25**, computed at the ωB97XD/6-311G(d,p) level.

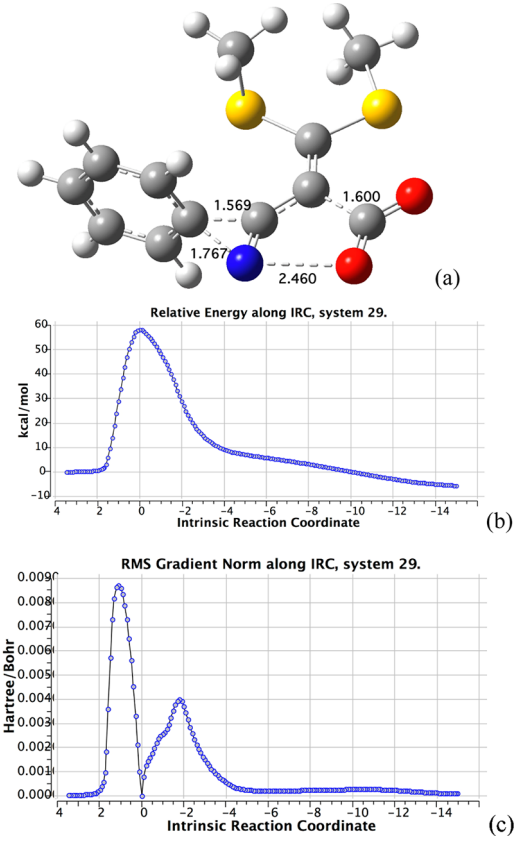

Figure 10. IRC profile for phenyl migration in **29**, yielding **32** (Scheme 3, path b), computed at the ωB97XD/6-311G(d,p) level. There is no evidence of either an explicit or a "hidden" intermediate corresponding to a nitrene **30** on this path.

The calculated barriers for both these processes are ~15 kcal/mol too high in relation to the estimated kinetics. We must therefore pause and ask whether the (closed shell) theoretical method is appropriate, since the probability of involving open shell electronic configurations must increase with barrier height. When the wave function at the computed geometry of the two transition states is subjected to a stability test toward open shell/UHF energy solutions, that for Figure 7b (methyl migration) is found to be stable, whereas Figure 7a (the azirene **23** pathway) has a triplet solution ~6 kcal/mol lower. An estimate of the singlet biradical barrier height can be obtained using a spin unrestricted broken-symmetry (UBS) approach.[19] This reduces the activation free energy of the azirene route from 64.3 to 62.1 kcal/mol, which may still be too high. An alternative way of assessing whether a single reference calculation is appropriate for a singlet species with some open shell (biradicaloid) character comes from a CASSCF(8,8) single-point calculation on both reactant and transition state for Figure 7a. The reactant reveals the closed shell electronic configuration (of 1764 considered) has a coefficient of 0.947, whereas this reduces to 0.815 for the transition state and the corresponding barrier drops by 7.6 kcal/mol to 57.3, which is in better agreement with the estimated experimental barrier. The closed shell DFT method thus overestimates the reaction barrier for transition states with biradicaloid character by perhaps 8−12 kcal/mol, while the spin-unrestricted (UBS) variation, sometimes used to study such species, reduces this only modestly. However, these errors are relatively small.

Whereas the barriers themselves for the two types of rearrangement are quite similar, the methyl migration (Figure 8a,b) is very slightly exothermic, but the azirene formation (Figure 8c,d) is highly endothermic.

In fact the formation of an azirene **23** is only part of a complex cascade. First, **23** cleaves a C−C bond with a tiny barrier to liberate CO_2. This species then cycloeliminates by extruding MeCN, concertedly with a final [1,2] hydrogen migration producing the alkyne **25** (Scheme 2 and Figure 9). These transition states are all lower in energy than the initial step, and hence are not rate limiting. The nitrene **22** and the vinylidene **24** are not present as either explicit or hidden intermediates; however, there is an instance of the latter (Figure 9b and Figure 9d marked with an arrow) that corresponds to a H-bridging vinylidene en-route to the alkyne **25**.

System 29 (Scheme 3). In **29** (Scheme 3), the simple H and aryl substituents in **21** have been replaced by methylthio groups, and the eventual product is di(methylthio)ethyne **28**, along with

dx.doi.org/10.1021/jo401146k | J. Org. Chem. 2013, 78, 7565−7574

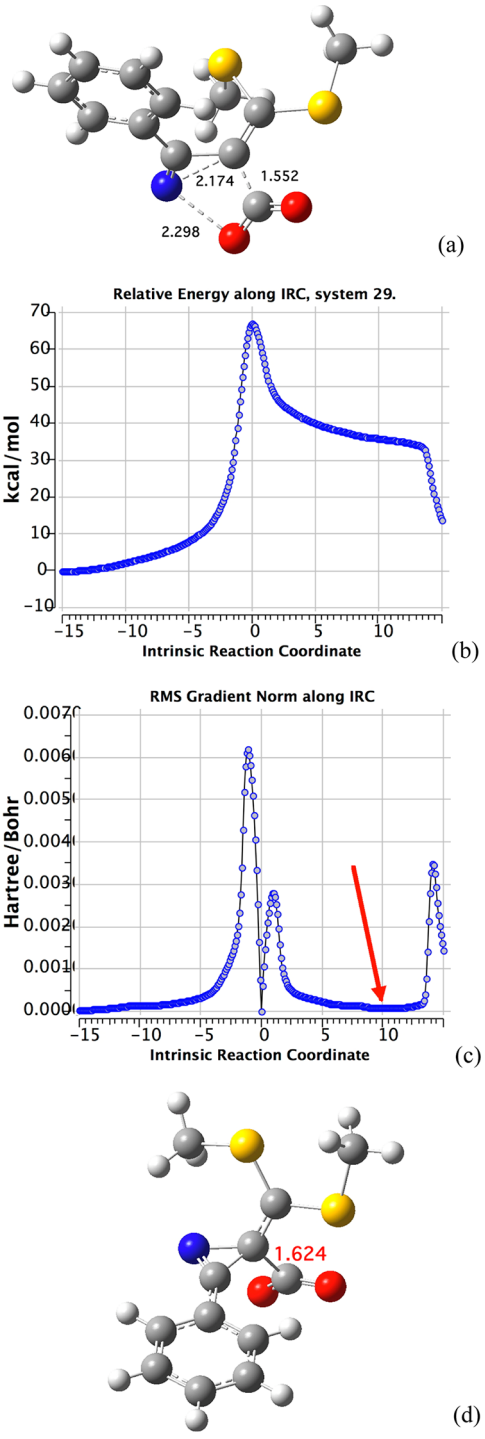

Figure 11. Transition state geometry (a), and IRC profile (b and c) for formation of azirene **31** from **29** (Scheme 3, path a) computed at the ωB97XD/6-311G(d,p) level, with (d) the geometry of the hidden zwitterionic intermediate, and its position is marked with an arrow in panel (c).

CO_2 and PhCN. The pathway (b) involving migration of the phenyl group, leading to cumulene **32**, is a closed shell pathway, but the route (a) involving elimination to form an azirene **31** is again unstable to a spin-unrestricted wave function. Route (a) forming **28** is the observed reaction. A CASSCF(8,8) single point calculation shows the primary closed shell configuration to the wave function to have a coefficient of 0.828 for the azirene trajectory and 0.946 for the phenyl migration, and leads to barriers of respectively 39.9 and 49.1 kcal/mol. This reverses the ordering obtained with the closed shell single-configuration DFT method and matches the experimentally observed formation of alkyne **28** as the product. There is no sign of any "hidden intermediate" corresponding to the nitrene **30** (Scheme 3 and Figure 10), but a hidden zwitterionic intermediate does appear on the azirene pathway (Figure 11c). Notably, a mechanism for converting the azirene **31** into the cumulene **32** could not be characterized, nor was there any experimental evidence for the formation of **32**.

Elimination of Me_2S from **29** affords the thioketene **33**, which sustains phenyl migration to form the cumulene PhNCCCS **36** directly, with no intervening intermediates, hidden or otherwise (Scheme 4, path a, and Figure 12). The alternative mechanism

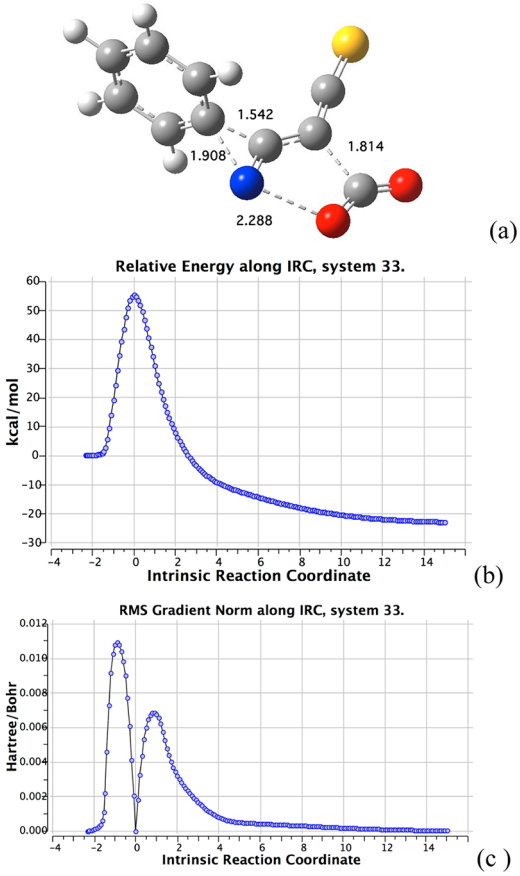

Figure 12. Transition state geometry (a), and IRC profile (b and c) for Ph migration in **33** leading to PhNCCCS **36** directly (Scheme 4, path a), computed at the ωB97XD/6-311G(d,p) level.

(Scheme 4, path b) involves a transition state 16.0 kcal/mol higher in free energy (closed shell DFT), or 12.2 kcal/mol higher at the CASSCF(8,8) level. As before, this route b bypasses the nitrene **34** as an explicit intermediate by leading directly to azirene **35**. Attempts to locate a transition state for the conversion of **35** to **36** led instead to extrusion of :C═C═S, the activation energy for this process being 20.0 kcal/mol lower than that for the formation of **35**. Thus the direct path a to the observed product PhNCCCS **36** is preferred.

In the ketenimine analogue **38** (Scheme 5) the computed free energy barrier again favors direct Ph migration to give PhNCCCNPh **59** rather than formation of the azirene **42**, by 13.2 kcal/mol (closed shell DFT) or by 6.8 [CASSCF(8,8)] (Figure 13). This is a rather smaller difference than the one described for **29**, and it leaves open the possibility that both

dx.doi.org/10.1021/jo401146k | J. Org. Chem. 2013, 78, 7565−7574

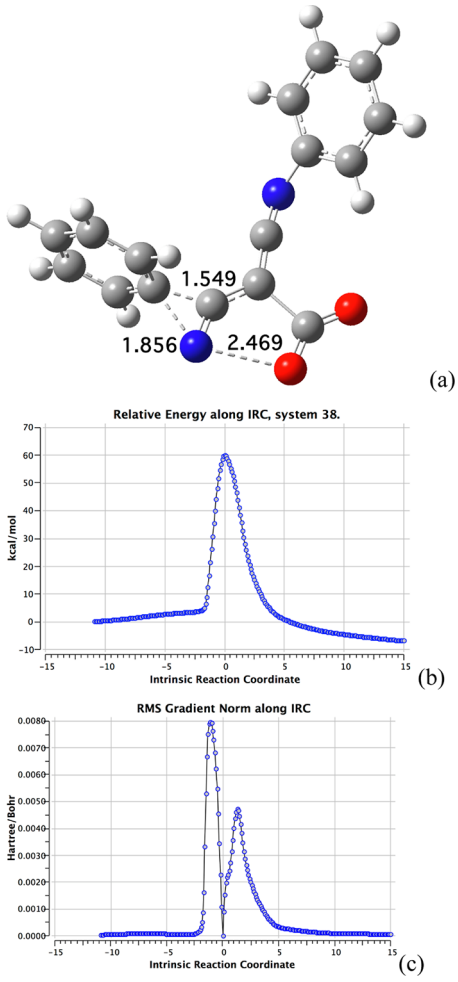

Figure 13. Transition state geometry (a), and IRC profile (b and c) for Ph migration in **38** computed at the ωB97XD/6-311G(d,p) level.

mechanisms may operate concurrently, in good agreement with the observation that **39** is the dominant product at 800 °C, but azirene **42** may be a fleeting intermediate in the intermediate temperature range as observed by mass spectrometry.

CONCLUSIONS

Modern computational quantum methodology such at that reported here is capable of performing a scan of a reasonably large set of reactions (Schemes 1−5) in a time that matches or is significantly shorter than that of the associated experimental laboratory work. Free energy barrier heights using dispersion-correction density functionals and a medium quality basis set are probably accurate to <10 kcal/mol, if not better,[20] which is normally accurate enough that mechanistic hypotheses can be subjected to quantitative scrutiny. For some types of high temperature/high barrier reactions, an encroachment into more highly correlated mechanisms in which biradicaloid character starts to manifest can be recognized, and simple corrections to the energy barriers can be estimated. The reactions studied here, ranging from those where the barrier is so low it prevents the synthesis of the reactants, to those where high temperatures are required, provide a good "stress-test" of this approach. Conventional mechanistic explorations using the type of "curly arrow pushing" taught in all introductory organic chemistry courses may not always provide insight into whether reactive species are explicit intermediates in such reactions, or whether the pathway avoids them entirely. Thus the reality of nitrene intermediates such as **17** or **22**, which might be assumed to be part of a mechanistic scheme, can be assessed and in these examples shown not to be involved. Intrinsic reaction coordinates can also reveal more transient "hidden intermediates", the participation of which might be useful information in designing variations to such reactions. Such quantitative mechanistic exploration should perhaps nowadays be considered a routine requirement for reporting new reactions, especially when the ranges of possible outcomes is so large and when so many intermediates in the mechanisms are merely inferred and not directly observed.

ASSOCIATED CONTENT

Supporting Information

A complete set of computational details, including input and output files, is available via a digital data repository, hyperlinks for which are included in the Web-enhanced-object (WEO) associated with Table 1. This material is available free of charge via the Internet at http://pubs.acs.org/doi/media/10.1021/jo401146k/index.html.

AUTHOR INFORMATION

Corresponding Author

*E-mail: rzepa@imperial.ac.uk (H.S.R); wentrup@uq.edu.au (C.W.).

Notes

The authors declare no competing financial interest.

ACKNOWLEDGMENTS

C.W. is indebted to the students and co-workers, whose names are given in the references.

REFERENCES

(1) Wentrup, C.; Finnerty, J. J.; Koch, R. *Curr. Org. Chem.* **2010**, *14*, 1586.
(2) Berstermann, H.-M.; Harder, R.; Winter, H.-W.; Wentrup, C. *Angew. Chem., Int. Ed. Engl.* **1980**, *19*, 564.
(3) Kappe, C. O.; Kollenz, G.; Wentrup, C. *Acta Chem. Scand.* **1993**, *47*, 940.
(4) In fact, green colorations of pyrolysates from isoxazolones have been observed on several occasions, thus hinting at the presence of nitroso compounds, but the quantities were too low to permit isolation of any definite substances.
(5) For the thermal ring opening of 1-azirene to open-shell singlet vinylnitrene, see: Nunes, C. M.; Reva, I.; Pinho e Melo, M. V. D.; Fausto, R.; Solomek, T.; Bally, T. *J. Am. Chem. Soc.* **2011**, *133*, 18911.
(6) For the thermal formation of azirenes, ketenimines, and acetonitriles from vinyl azides (vinyl nitrenes), see: (a) Hassner, A.; Wiegand, N. H.; Gottlieb, H. E. *J. Org. Chem.* **1986**, *51*, 3176. (b) Banert, K.; Fotsing, J. R.; Hagedorn, M.; Reisenauer, H. P.; Maier, G. *Tetrahedron* **2008**, *64*, 5645.
(7) Wentrup, C.; Stutz, U.; Wollweber, H.-J. *Angew. Chem., Int. Ed. Engl.* **1978**, *17*, 688.
(8) The same method can be used to generate fulminic acid (HCNO), organic fulminates (RONC), and isocyanamins (RR′N−NC): (a) Wentrup, C.; Gerecht, B.; Briehl, H. *Angew. Chem., Int. Ed. Engl.* **1979**, *18*, 467. (b) Wentrup, C.; Gerecht, B.; Laqua, D.; Briehl, H.; Winter, H.-W.; Reisenauer, H. P.; Winnewisser, M. *J. Org. Chem.* **1981**, *46*, 1046. (c) Wentrup, C.; Winter, H.-W. *J. Org. Chem.* **1981**, *46*, 1045.
(9) Wentrup, C.; Winter, H.-W. *Angew. Chem., Int. Ed. Engl.* **1978**, *17*, 609.
(10) The same method can be used to generate ethynylamines, ketenimines, and acetonitriles: Wentrup, C.; Briehl, H.; Lorenzak, P.;

Vogelbacher, U.; Winter, H.-W.; Maquestiau, A.; Flammang, R. *J. Am. Chem. Soc.* **1988**, *110*, 1337.
(11) Schulenburg, W.; von der, Graf; Hopf, H.; Walsh, R. *Angew. Chem., Int. Ed.* **1999**, *38*, 1128. Ebrahimi, A.; Deyhimi, F.; Roohi, H. *J. Mol. Struct.: THEOCHEM* **2001**, *246*, 207.
(12) Kvaskoff, D.; Wentrup, C. *Aust. J. Chem.* **2010**, *63*, 1694.
(13) Wolf, R.; Stadtmüller, S.; Wong, M. W.; Flammang, R.; Barbieux-Flammang, M.; Wentrup, C. *Chem.—Eur. J.* **1996**, *2*, 1318.
(14) Chai, J.-D.; Head-Gordon, M. *Phys. Chem. Chem. Phys.* **2008**, 6615.
(15) Downing, J.; Murray-Rust, P.; Tonge, A. P.; Morgan, P.; Rzepa, H. S.; Cotterill, F.; Day, N.; Harvey, M. J. *J. Chem. Inf. Model.* **2008**, *48*, 1571.
(16) Rzepa, H. S. *J. Chemoinf.* **2013**, *5*, 6.
(17) Whitesides, G. In *Publishing Your Research 101: Impact of Technology on Scientific Articles*; American Chemical Society: Washington, D.C., 2011; http://www.youtube.com/embed/NHuC5yZeHYQ (accessed 24 May, 2013).
(18) Cremer, D.; Kraka, Elfi. *Acc. Chem. Res.* **2010**, *43*, 591−601.
(19) See, for example: Chen, Z.; Jiang, D.; Lu, X.; Bettinger, H. F.; Dai, S.; Schleyer, P. von R.; Houk, K. N. *Org. Lett.* **2007**, 5449−5452.
(20) For another typical example of mechanistic exploration at this theoretical level, see: Buchard, A. P.; Jutz, F.; Kember, F. M. R.; Rzepa, H. S.; Williams, C. K. *Macromolecules* **2012**, *45*, 6781−6795.